10.2352/EI.2022.34.15.COLOR-375

Printed paper-based devices for detection of food-borne contaminants: New device design and new colorimetric image analysis methods

Qiyue Liang [1], *Min Zhao* [1], *Ana Maria NA Ulloa Gomez* [2], *George T. C. Chiu* [3], *Lia A Stanciu* [2], *Amanda J Deering* [4], *and Jan P. Allebach* [1]
[1] *School of Electrical and Computer Engineering, Purdue University, West Lafayette, IN, USA*
[2] *School of Materials Engineering, Purdue University, West Lafayette, IN, USA*
[3] *School of Mechanical Engineering, Purdue University, West Lafayette, IN, USA*
[4] *Department of Food Science, Purdue University, West Lafayette, IN, USA*

Abstract

In this paper, we introduce a paper-based microfluidic device design that allows liquids to flow at a constant rate through the channels. The device pattern is designed based on a flow rate control test. Our proposed device can be easily manufactured by a wax printer and be printed on filter paper. The primary function of the paper device is to measure the concentration of hazardous chemicals such as heavy metals and bacteria in liquids. We also propose two new image analysis metrics, hue difference and chroma magnitude difference, for analyzing the color of images as a means of identifying the concentration of heavy metals in solutions. In addition, we discuss in detail the image processing pipeline for analyzing the devices from the initial image capturing to segmentation and analysis. This paper also discusses future goals and possible directions to take, such as handling the device from different viewpoints.

Introduction

A paper-based device is frequently found in a variety of locations for use on a daily basis. The use of paper based microfluidic devices is often driven by their inexpensiveness and ease of use. There is nothing uncommon about coming up with a random device design that might have any kind of strange shape, but how do we determine if it is a good design? In our case, we are concerned with ensuring that the liquids are flowing at equal flow rates through all of the channels in our device. This is due to the fact that our purpose is to design a paper device that can detect multiple foodborne contaminants at once, so we need multiple channels and constant flow rates. Based on the requirement of equal flow rates, we propose a new design layout. Our proposed paper device is intended to be used by people in the field, such as testing the concentration of harmful chemicals contained in suspicious food items of a grocery store. Since there are a lot of uncertainties in real life situations, we need to make sure that the devices are functional. Therefore, we use four different types of colorimetric quantification methods in order to ensure that, if one of them is successful, we can proceed. Specifically, the four methods are: CIE 1976 Delta E, Chroma, Hue Difference, and Chroma Magnitude. The first two methods are already widely used under many different circumstances, and the latter two methods are our proposed new colorimetric image analysis methods to help us determine the color difference of our paper devices. Details of these methods are shown in colorimetric image analysis methods section of this paper.

Related Works

In this paper, we mainly focus on testing the concentration of Hg^{2+} ions to illustrate how to use our paper devices and demonstrate our colorimetric analysis results. The details about how the Hg^{2+} ions react with the target and the underlying mechanism of how this reaction affects the color of the target are described in [1], which was a paper published earlier by the materials science group that collaborates with us on this project. Although in this paper, the scope of testing using our proposed device is primarily focused on heavy metals, it can easily be extended to testing other harmful chemicals and food borne pathogens [2], [3]. Previous work by our group has proposed a paper device with four channels for measuring the concentration of heavy metal particles [4]. The difference between our previous work and the current one is that previously we used screen printing to fabricate the device, and the entire device dimension was larger (45 mm x 45 mm). Now, we are using wax printing, which has higher resolution, is easier to fabricate, and the fabricated device has smaller dimensions as shown in device design part of this paper. Detailed explanations of the wax printing process used to fabricate our paper device are provided in the following paper [5]. We are not the first group to use wax printing to fabricate paper based devices. This technique has been used by a number of other groups [6], [7], [8]. As we stated earlier, when we are dealing with the design of the device, we are considering equivalent flow rates in all channels of our device. We discovered that a Y-shaped device is useful in controlling flow rate [9], [10], so we updated our device design accordingly. Our ultimate goal is to design a paper device that can easily be used on a daily basis, which means that, in real life, the picture of the device may be taken from a different perspectives. In order to compensate for the perspective difference and return the device to its rightful position, we may add extra features to the device to help us calculate the homography and restore the picture to the front position. One method is to use Aruco markers [11] to track the corners of the device and calculate the homography based on those corner coordinates.

Experimental Preparations

Device Design

One of the primary advantages of wax printing is that the process is very straightforward. Fabrication of our wax printing paper device involves two steps: the first step is to print the wax pattern using a Xerox ColorQube 8570 wax printer (Rochester, NY, USA) on Whatman Grade 1 filter paper (Milwaukee, WI, USA); the next step is to melt the wax pattern with a heat gun (Maxwel Manufactoring, Victoria, Australia). More details concerning wax pattern fabrication and printer calibration can be found in the paper published by our group earlier [5]. Prior to this time, we were designing and prototyping preliminary devices, and now we are working with our colleagues in materials science. As shown in Figure 1(a), it has been found that the flow rate through the multi channel paper device is not equal in all channels when our materials science colleagues are conducting the experiments.

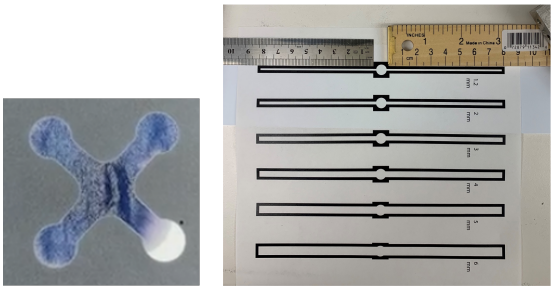

(a) (b)

Figure 1: (a) An example of our previous wax pattern having unequal flow rates, (b) Wax printed channels of varying widths (from 1.2 mm to 6 mm) designed for flow rate control.

As a result of experimental challenges that our material science colleagues have faced, we must adapt the device dimensions and the overall configuration to equalize the flow rates in all channels. For the purpose of finding the optimal channel width, we design the patterns as shown in Figure 1(b). Wax printed channels with a width ranging from 1.2 mm to 6 mm are fabricated, and solutions are dropped through the middle circle. The channels are 80 mm long on each side. Once the liquid has entered the channels, we measure the distance and time it takes for the liquid to flow. The results of the flow rate control are shown in Figure 2 (b). Flow rates are recorded for each channel width, both on the left and on the right hand side of the channels. The two data points at each time tick mark reflect the flow distance of the liquid in the left channel and the right channel at the time they are recorded. What is important is that there should be equal flow rates both side of the channels. And it can be observed that for the 2 mm channel, the flow rates in the left and right channels are approximately equal, because the two data points on each time tick are close to one another. Also, it is noticeable that the liquid flows the fastest through the 4 mm channels, but the flow rates on the left and right sides of the channel are not quite equal. There is no change in the last few data points of the 4 mm channel since the total channel length is 80 mm and the liquids have already reached the end of the channel. Therefore, 2 mm channel width is preferable when we design our devices since we desire even flow rates in all channels, but are not very concerned about how fast the liquid flows. Additionally, it was noticed that the liquid flowed on top of the paper surface rather than wicking through the filter paper, which may also result in an uneven flow rate. Thus, we considered designing a geometry that would allow the liquid to flow through wicking. Following these guidelines, we designed our new device pattern shown in Figure 2 (b). The new device is much smaller than the previous pattern. The main channel measures 2 mm in width, and the circle diameter measures 4.3 mm. In the previous pattern, the circles are 8 mm in diameter and the channels are 4 mm wide. The new design adds an extra circle to the pattern on the left hand side, as shown in Figure 2(b). The extra circle does not connect to any channels. It should be left blank during the experiment and will serve as a white reference for each device in the image analysis pipeline. The inlet of this device is the smaller circle to the middle right. This is a four channel device, the reason we add an extra inlet circle and channel is because we find that if we drop the solution on the middle right circle rather than directly on the center of the channel at a point that is equidistant from the four circles, the middle right circle will act as a reservoir, and the solution will slowly be wicked away by the channel rather than rushed into it.

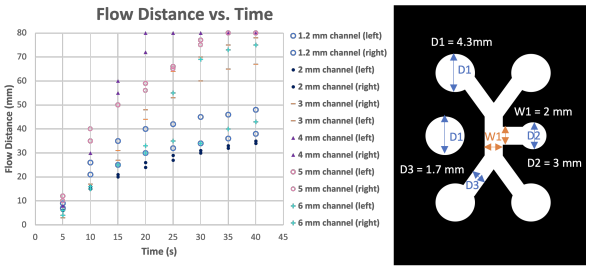

(a) (b)

Figure 2: (a) Results of flow rate tests in six channels with varying widths from 1.2 mm to 6 mm, using the devices shown in Figure 1(b), (b) New pattern with configuration details.

Picture Taking Settings

Our colleagues in the material sciences use our fabricated paper devices for conducting experiments to measure the concentration of heavy metal particles. It is important to properly take pictures of the devices after the experiments are completed in order to prepare them for image analysis. As illustrated in Figure 3(a), we take our photos in a photo booth (Zecti Photo Box, Shenzhen, China) under fixed lighting conditions, which is the same setting as in our previous publication [4]. A 45 degree angle holder was established in the photo booth to assist us when handing our paper devices. Photographs are taken with a mobile phone that is perpendicular to the paper holder and at a fixed distance from the paper holder. In order to ensure that we are taking pictures from the same distance each time, we use a tripod (Manfrotto Compact Advanced Aluminum Tripod, Cassola, Italy) to hold the phone and record the tripod's position. As shown in Figure 3(b), a mobile phone application called *Manual is used to control the mobile phone camera settings. In order to identify the best parameters for taking pictures, we alter the settings on the app and take pictures using different settings. Figure 3(c) shows pictures taken under several different settings, and the RGB values on the bottom white reference circle are calculated to ensure that the photographs are not overexposed. When they are overexposed, at least one RGB value will be close to 255. After photo capturing, the photos will*

be used in the image processing pipeline to determine the particle concentration.

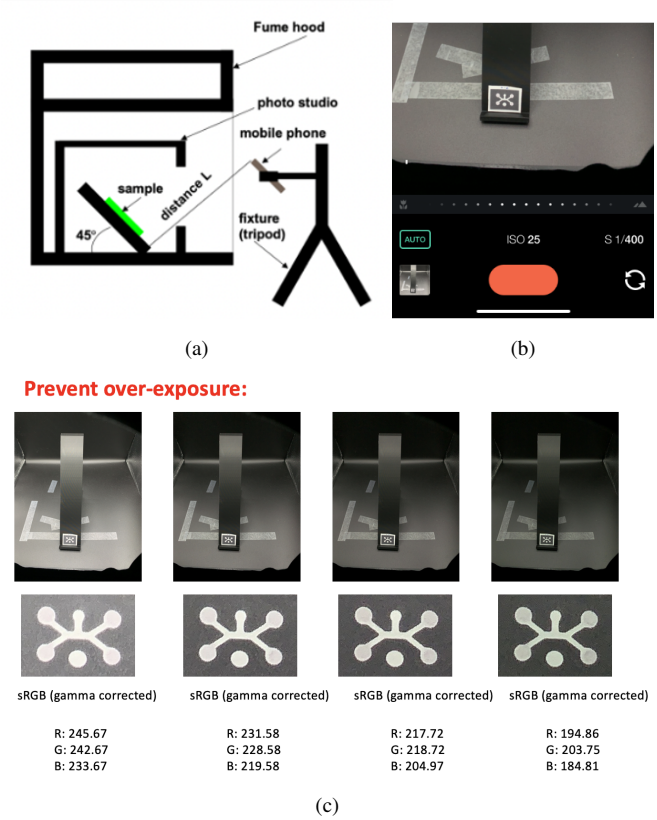

(a) (b) (c)

Figure 3: (a) To take pictures in a photo booth, we use the same setting as in our previous publication [4], (b) To keep the same parameters, pictures are taken using an app called Manual, (c) Varying the camera settings to prevent overexposure.

Data Analysis

Image Processing Pipeline

There may be more than one device in the same picture. In this case, we must first locate all devices using template matching. For the template, we can select one of the devices. All other devices will be matched to the selected device and cropped with the same dimensions. Once a device is detected, a white mask is applied to the device area to prevent it from being detected more than once. Upon detection of all devices as shown by green boxes in Figure 4, each device will be analyzed individually.

The image processing pipeline for each device is shown in Figure 5. We first calculate CIE 1976 delatE from the original image, and then get an image that looks grayscale. Using the Delta E image, we then perform a 4-cluster k-means[12]. We choose four clusters because in the original unprocessed image, there are channels that contain one color, pads that contain a second color, and the background that contains two more colors. We assign two colors to the background because it is not exactly uniform. This four cluster k-means is used as a preliminary segmentation method. Immediately following the preliminary 4 cluster k-means, we remove the parts of the image that pertain to the background and perform another 3 cluster k-means on just the channel and pads area. Three clusters are used for this step since the channel

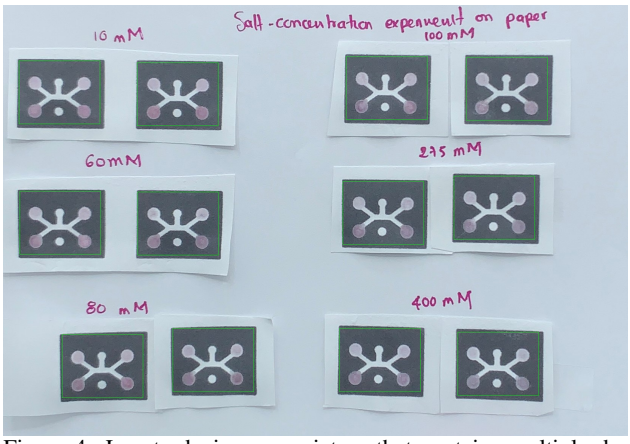

Figure 4: Locate device on a picture that contains multiple devices.

area contains one color, whereas the pad area may contain one to two colors, depending on whether or not the color in the pad is uniform, for example if there is a coffee ring. This three cluster k-means procedure is used to separate the channel area from the pad area. Next, we create a mask using the same regions that were used for the 3 cluster k-means. This mask is formed for the purpose of cropping the regions of interest, namely the pads and channels. The mask, however, is too large and includes unnecessary areas, such as the noisy outline of the pads. As a result, we apply a morphological erosion of 20 pixels by 20 pixels to remove the outer parts of the mask, which also eliminates the coffee ring if there is one. Then, we apply the eroded mask to the previous 3 cluster k-means result to produce the final segmentation. Only those parts that are both within the mask and also belong to the pad area in the 3 cluster k-means result are included. In the final segmentation, there should be four pads. The bottom white reference circle is not included. This is because the color of the white reference circle is light, which is similar to the color of the channels that are not treated by the analytes, which are designed to change color when exposed to the target contaminant. Due to the similar colors of the white reference and the channel areas, the white reference is grouped into the same cluster as the channel areas when 3 cluster k-means was performed. As the final segmentation contains four pads, we can determine the location of each pad using spatial information.

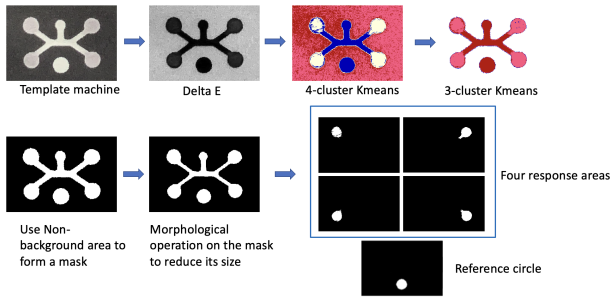

Figure 5: The image processing pipeline to analyze each device.

Colorimetric Image Analysis Methods

Once we have located all four pads, we may proceed to perform colorimetric image analysis on the pad areas we have identi-

fied. Pre-dropped solutions on the pads will change color depending on the concentration of heavy metal particles. Calculating the CIE Delta E between two color patches is a common method of assessing colorimetric differences. The Delta E is calculated in this case by comparing the four circular pads with the white reference pad at the bottom. The Delta E we are referring to is the CIE 1976 Delta E as shown in Equation 1, as it is a standard among many companies. Nonetheless, there are also more recent definitions of Delta Es which we may examine as well. Another very common measurement is Chroma (Equation), which does not take into account the lighting in the Delta E calculation.

$$CIE\ 1976\ \Delta E_{a^*b^*} = \sqrt{(L_1^* - L_1^*)^2 + (a_1^* - a_2^*)^2 + (b_1^* - b_2^*)^2} \tag{1}$$

$$Chroma\ Difference = \sqrt{((a_1^* - a_2^*)^2 + (b_1^* - b_2^*)^2}$$

In addition to the traditional image analysis methods, we define two new methods which can be used to identify color differences. We name the two new methods as Hue difference and Chroma magnitude difference. Hue difference can be defined as follows: if we have two points on the CIE a b* plane, Hue difference is the angle between the two lines joining the points on the a* b* plane to the origin of the a* b* plane. We may in this case consider one a*b* value to correspond to the testing area and the other a*b* value to correspond to the white reference area. The final Hue difference is calculated by averaging all angles. As for the Chroma magnitude difference, it is simply the difference in length between the two lines connecting the points on the a* b* plane to the origin of the a* b* plane. The final Chroma magnitude difference is also an average of all Chroma magnitude differences. For an intuitive understanding of these two new image analysis methods, we generate a graph as shown in Figure 6.*

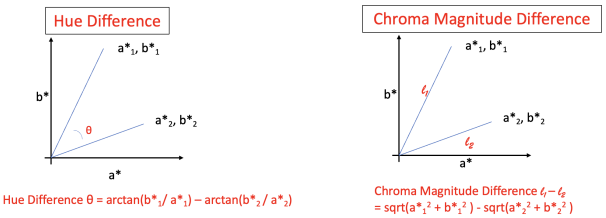

Figure 6: Hue difference and Chroma magnitude difference

Figure 7 illustrates the results of employing all four color analysis methods on one batch of the devices. In this batch, there are five devices for each concentration, and each device consists of four pads. As a result, we have 20 data points for each concentration, corresponding to four pads times five devices. It is ideal to obtain a result with a monotonic trend and with good separation between each concentration of heavy metals. We can see in the four graphs that the Chroma magnitude indicates a decreasing trend for the lower concentrations, 0 to 20 ppm. This trend is less evident in the other metrics. Consequently, it is vital that our pictures be analyzed using a variety of metrics, since if we use only one metric, we may miss trends that could be identified using other metrics.

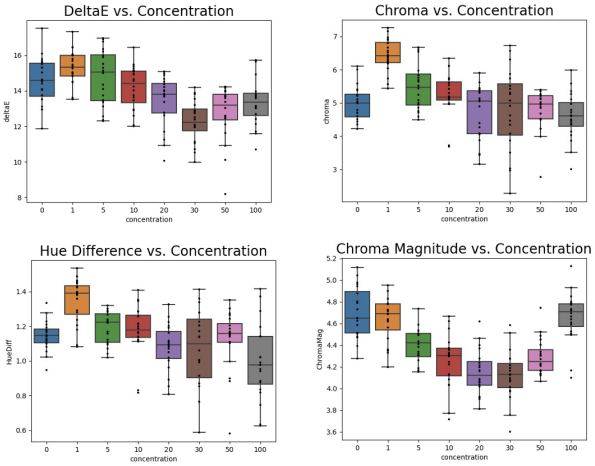

Figure 7: Analysis results of one batch of devices using tradiational and new image analysis methods.

Color analysis with other methods

As an alternative to segmenting the pad areas and performing a colorimetric image analysis, we may also use a spectroradiometer to evaluate the differences in reflectance between the pads. As shown in Figure 8(a), we use the PhotoResearch spectroradiometer PR-705 (Reno, Nevada, USA) to capture the reflectance of the reaction pad areas. Since the spectral radiometer is extremely sensitive to outside light, the entire experiment should be conducted in complete darkness. The spectroradiometer is first used to measure the spectral radiance of a white reflectance target (Figure 8(b), which is a small disk that may serve as the white reference. We then measure the spectral radiance of each circular pad within the devices, as shown in Figure 8(c). If we divide the spectral radiance of each pad by the spectral radiance of the white reflectance, we can calculate the reflectivity. We select the region of the reflectivity curve that shows the greatest separation as shown in Figure 8(d), and we only evaluate the images within this region. It should be noted that this method is different from the previous method, which made use of segmentation, Delta E etc., but it is also considered a traditional evaluation metric.

Future Goals and Other Ideas

Our ultimate goal to develop a mobile application that will enable people in the field, such as employees in a grocery store, to detect the concentration of food-borne contaminants. In case that people come across food items that are suspicious, we want them be able to quickly and easily perform tests using these low-cost devices, which is why we are planning on developing a mobile app. In order to achieve our ultimate goal, we need to enable people taking pictures in different directions. One method for doing so is by adding patterns to the device that can help adjust the picture to the desired view. Aruco markers of size 6x6 are added to the corners of the device pattern, as shown in Figure 9(a) and Figure 9(b). We use four distinct markers to identify which corner is which. These Aruco markers can be identified from the picture, and their indexes are used to calculate the homography, which can reverse the picture back to the front view, as shown in Figure 9(c).

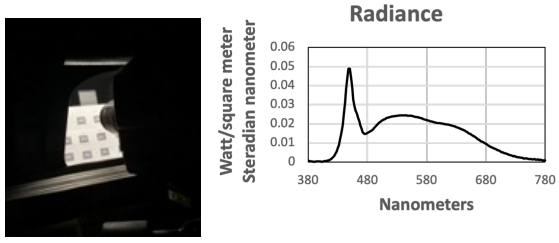

(a) (b)

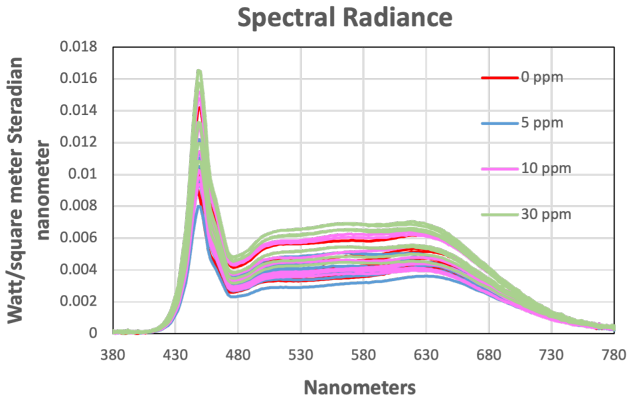

(c)

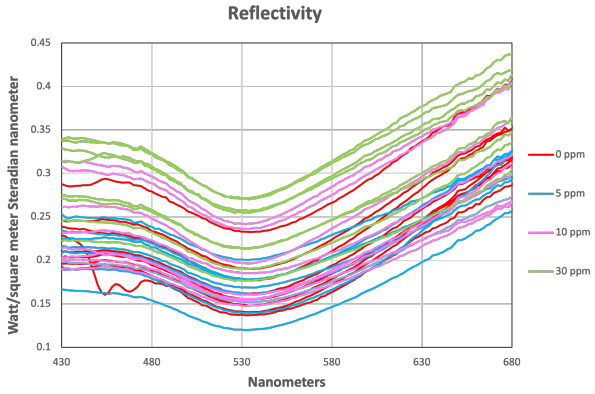

(d)

Figure 8: (a) We set up the spectroradiometer in darkness, (b) We use spectroradiometer to measure the radiance of white reflectance, (c) We use spectroradiometer to measure the spectral radiance of each pad within the device, (d) We divide the radiances of the pads by the radiance of the white reflectance to obtain the reflectivity.

Conclusion

In this paper, we present a new multi-channel paper based microfluidic device fabricated by wax printing. This new design is aimed at ensuring equal flow rates in all channels of the paper device. Our new device design was developed based on flow rate control experiments. The new design has smaller dimensions than our previous device, so it can reduce the volume of chemical solutions when doing experiments. We carefully optimize the picture taking settings and image processing pipelines to capture the pad areas of the devices where the chemical reactions between heavy metal particles and the detection target take place. Two new image analysis metrics, Chroma Magnitude Difference and Hue Difference, were proposed to evaluate colorimetric responses of the pad areas. We also use traditional image analysis metrics, including Delta E, chroma, and spectral radiance to assess the color differences between our devices. At the end, we briefly discuss future goals and other items that we can add to the device to enhance its functionality.

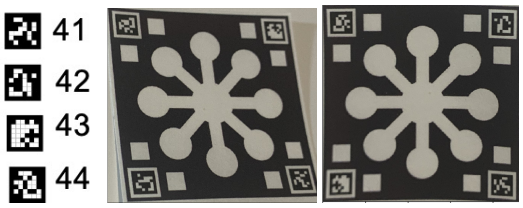

(a) (b) (c)

Figure 9: (a) The four Aruco markers we use, (b) Picture of the device that is tilted, (c) Reversal of the tilted device to front view using the four Aruco markers.

Acknowledgments

This manuscript is based upon work supported by the U.S. Department of Agriculture, Agricultural Research Service, under Agreement No. 59-8072-6-001. Any opinions, findings, conclusion, or recommendations expressed in this publication are those of the author(s) and do not necessarily reflect the view of the U.S. Department of Agriculture.

References

[1] *S. Díaz-Amaya, M. Zhao, J. P. Allebach, G. T.-C. Chiu, and L. A. Stanciu, "Ionic strength influences on biofunctional au-decorated microparticles for enhanced performance in multiplexed colorimetric sensors,"* ACS Applied Materials & Interfaces, *vol. 12, no. 29, pp. 32397–32409, 2020.*

[2] *S. Díaz-Amaya, M. Zhao, L.-K. Lin, C. Ostos, J. P. Allebach, G. T.-C. Chiu, A. J. Deering, and L. A. Stanciu, "Inkjet printed nanopatterned aptamer-based sensors for improved optical detection of foodborne pathogens,"* Small, *vol. 15, no. 24, p. 1805342, 2019.*

[3] *M. Zhao, S. Diaz Amaya, S.-a. Jin, L.-K. Lin, A. J. Deering, L. Stanciu, G. T.-C. Chiu, and J. P. Allebach, "Inkjet printing platforms for dna-based pathogen detection," in* NIP & Digital Fabrication Conference, *vol. 2018, pp. 107–112, Society for Imaging Science and Technology, 2018.*

[4] *M. Zhao, S. Diaz-Amaya, A. J. Deering, L. Stanciu, G. T.-C. Chiu, and J. P. Allebach, "Image analytics for food safety,"* Electronic Imaging, *vol. 2020, no. 8, pp. 302–1, 2020.*

[5] *Q. Liang, M. Zhao, G. T. Chiu, and J. P. Allebach, "Design and fabrication of microfluidics paper-based devices for contaminant detection using awax printer,"* Electronic Imaging, *vol. 2021, no. 16, pp. 339–1, 2021.*

[6] *E. Carrilho, A. W. Martinez, and G. M. Whitesides, "Understanding wax printing: a simple micropatterning process for paper-based microfluidics,"* Analytical chemistry,

vol. 81, no. 16, pp. 7091–7095, 2009.

[7] G. G. Morbioli, N. C. Speller, M. E. Cato, T. P. Cantrell, and A. M. Stockton, "Rapid and low-cost development of microfluidic devices using wax printing and microwave treatment," Sensors and Actuators B: Chemical*, vol. 284, pp. 650–656, 2019.*

[8] M. Younas, A. Maryam, M. Khan, A. A. Nawaz, S. H. I. Jaffery, M. N. Anwar, and L. Ali, "Parametric analysis of wax printing technique for fabricating microfluidic paper-based analytic devices (μpad) for milk adulteration analysis," Microfluidics and Nanofluidics*, vol. 23, no. 3, pp. 1–10, 2019.*

[9] I. Jang and S. Song, "Facile and precise flow control for a paper-based microfluidic device through varying paper permeability," Lab on a Chip*, vol. 15, no. 16, pp. 3405–3412, 2015.*

[10] J. L. Osborn, B. Lutz, E. Fu, P. Kauffman, D. Y. Stevens, and P. Yager, "Microfluidics without pumps: reinventing the t-sensor and h-filter in paper networks," Lab on a Chip*, vol. 10, no. 20, pp. 2659–2665, 2010.*

[11] S. Garrido-Jurado, R. Muñoz-Salinas, F. J. Madrid-Cuevas, and M. J. Marín-Jiménez, "Automatic generation and detection of highly reliable fiducial markers under occlusion," Pattern Recognition*, vol. 47, no. 6, pp. 2280–2292, 2014.*

[12] J. A. Hartigan and M. A. Wong, "Algorithm as 136: A k-means clustering algorithm," Journal of the royal statistical society. series c (applied statistics)*, vol. 28, no. 1, pp. 100–108, 1979.*

Author Biography

Qiyue Liang is pursuing a Ph.D degree in electrical engineering at Purdue University under the supervision of Professor Jan P. Allebach. She received her B.S of science in electrical engineering degree from Purdue University(2018). Her current research interests include image processing and machine learning.